Growth rate effect on microstructure and thermoelectric properties of melt grown $Bi_2Ba_2Co_2O_x$ textured ceramics

Sh. Rasekh[1], G. Constantinescu[1], M. A. Torres[2], M. A. Madre[1], J. C. Diez[1], A. Sotelo[1]

[1] Instituto de Ciencia de Materiales de Aragón (CSIC-Universidad de Zaragoza), Mª de Luna, 3. 50018 Zaragoza, Spain.

[2] Departamento de Ingeniería de Diseño y Fabricación, Universidad de Zaragoza, Mª de Luna, 3. 50018 Zaragoza, Spain.

Abstract

$Bi_2Ba_2Co_2O_x$ thermoelectric ceramics have been grown from the melt, using the laser floating zone method, at different growth rates (15, 30 and 90 mm/h). Microstructure has shown an improvement on the grain alignment and a reduction of secondary phases when the growth speed is decreased. These microstructural features have been reflected on the thermoelectric performances, with a reduction on the electrical resistivity and, as a consequence, an important increase on the power factor values, reaching ~0.15 $mW/K^2.m$ at 650 ºC for samples grown at 15 mm/h, much higher than the typical values obtained in this materials.

I. INTRODUCTION

Thermoelectric (TE) energy conversion has been shown as an effective technology that can be used to transform directly thermal to electrical energy without moving parts or other dissipative systems. Nowadays, TE power generation technology is regarded as one of the most promising methods to harvest energy from different natural and/or wasted heat sources. Furthermore, these materials can be also applied in classical energy transformation systems improving their efficiency. As a consequence, this promising technology would help to reduce CO_2 emissions in energy generation. On the other hand, TE materials with high-energy conversion efficiency are strongly required for electric power generation before they can be considered for practical applications. The performances of these type of materials are quantified by the dimensionless figure of merit, ZT, which is defined as $TS^2/\rho\kappa$ (where S is the Seebeck coefficient, T the absolute temperature, ρ the electrical resistivity and κ the thermal conductivity). From this definition, it can be easily deduced that a high performance TE material should possess a high Seebeck coefficient (or thermopower), with low electrical resistivity and thermal conductivity.[1]

For the past two decades, intermetallic materials such as semiconductors, with high ZT, have been widely applied in various industrial and/or nonindustrial sectors, e.g. automobile industry (mainly in exhaust system). Nonetheless, these materials have some drawbacks as low stability at high temperature, which can result in degradation, oxidation, and/or evaporation. Moreover, usually they are mainly composed of heavy and/or toxic elements. This situation has changed in 1997, by the discovery of large TE properties in Na_xCoO_2.[2] Since then, great efforts have been performed to explore new TE materials, especially in the CoO-based families, with high TE performances. These research works led to the discovery of new layered cobaltites, such as $[Ca_2CoO_3][CoO_2]_{1.62}$ and $[Bi_{0.87}SrO_2]_2[CoO_2]_{1.82}$ with promising TE properties.[3-7]

The cobaltites crystal structure is formed by two different layers, which can be described as an alternate stacking of a common conductive CdI_2-type CoO_2 layer with a two-dimensional triangular lattice, and a block layer, composed of insulating rock-salt-type (RS) layers. The two sublattices (RS block and CdI_2-type CoO_2 layer) possess common

a- and c-axis lattice parameters and β angles while they have different b-axis length, causing a misfit along the b-direction.[7-10]

As a consequence of their crystal structure, layered cobaltites possess a very high crystallographical anisotropy which, in turn, produces a high electrical one. For this reason, the alignment of their plate-like grains, by mechanical and/or chemical processes, is essential to attain macroscopic properties comparable to those obtained on single crystals. Some methods have been shown to be adequate to obtain a good grain orientation in several oxide ceramic systems, as template grain growth (TGG),[11] sinter forging,[12] spark plasma sintering,[13] or directional growth from the melt.[14] All texturing techniques produce well oriented grains, leading to the reduction on the electrical resistivity. On the other hand, it is usual that the decrease on the resistivity is accompanied, at least in the solid state texturing methods, by a reduction of Seebeck coefficient values. When considering one of the directional growth from the melt methods, the laser floating zone (LFZ), it has shown a high reliability to obtain a good grain orientation in thermoelectric ceramic systems.[14] Moreover, due to the high thermal gradient produced in the solidification interface, it can produce textured ceramics at higher rates than the usual in other melt growth systems. As a consequence, the samples grown by this technique show a reduction of electrical resistivity, but usually lower than expected due to the simultaneous secondary phases formation.[15] On the other hand, previous studies on laser grown samples have shown that the textured samples produced by this technique possess, at the same time, higher Seebeck coefficient values than usual in these systems due to the raise on the oxygen vacancies.[16] In this context, the aim of the present study is studying the effect of growth rate on the microstructure and TE properties of $Bi_2Ba_2Co_2O_x$ textured ceramics fabricated by the LFZ technique.

II. EXPERIMENTAL

The $Bi_2Ba_2Co_2O_x$ polycrystalline samples used in this work were prepared using the classical solid-state route from commercial Bi_2O_3 (Panreac, 98 + %), $BaCO_3$ (Panreac, 99 + %), and Co_2O_3 (Aldrich, 98 + %) powders. They were weighed in the appropriate proportions, mixed and ball milled in acetone media at 300 rpm for 30 minutes to

produce a homogeneous mixture. The powders suspension in acetone was then dried in an IR evaporation system until total acetone evaporation. The remaining powder was manually ground and thermally treated twice, in an electrical furnace under air, at 750 and 800 ºC for about 12 hours, with an intermediate manual milling. The main objective of this process is assuring the barium carbonate complete decomposition. Otherwise, it would decompose in the molten zone, producing the formation of CO_2 bubbles inside the melt produced in the LFZ melt texturing process, leading to the crystallization front destabilization. The thermally treated powders were then milled, introduced into a latex tube (inner diameter ~ 3mm), and isostatically cold pressed at 200 MPa for around one minute to obtain green ceramic cylinders which were subsequently used as feed in a LFZ device equipped with a continuous power Nd:YAG laser (1.06 μm) and described elsewhere.[17]

All the growth processes were performed in the same conditions except for the different used growth rates (15, 30, and 90 mm/h). All the samples were grown downwards with a seed rotation of 3 rpm anticlockwise. Moreover, in order to assure compositional homogeneity of the molten zone, an opposite feed rotation of 15 rpm, clockwise, has also been performed. After the texturing process, long (more than 15 cm) and geometrically homogeneous (~ 2 mm diameter) textured cylindrical rods have been produced. Finally, the textured bars were cut into pieces with the adequate dimensions for their thermoelectric characterization (~ 15 mm long pieces).

The structural characterization, as well as the identification of the main phases in all textured samples has been carried out using powder XRD in a Rigaku D/max-B X-ray powder diffractometer (CuKα radiation), between 5 and 60 degrees. Microstructures have been observed using a scanning electron microscope (JEOL 6000) equipped with an energy dispersive X-ray spectroscopy (EDS) device that was used to determine the elemental composition of each identified phase. Longitudinal polished sections of all the textured samples have been observed to determine the microstructural evolution of the samples with the growth speed. Moreover, it has allowed the identification of the different phases and their distribution. Image analysis has been performed on several micrographs for each growth rate in order to estimate the volume fraction of each phase as a function of the growth speed. Thermoelectric properties, electrical resistivity and

Seebeck coefficient, were simultaneously determined by the standard dc four-probe technique in a LSR3 measurement system (Linseis GmbH) under He atmosphere, in the steady state mode, at temperatures ranging from 50 to 650ºC. In order to determine the samples performances, power factor (PF, defined as S^2/ρ) has been calculated from the measured electrical resistivity and Seebeck coefficient data.

III. RESULTS AND DISCUSSION

Powder XRD patterns for the $Bi_2Ba_2Co_2O_x$ (222) samples grown at different rates are displayed (from 10 to 40 degrees, for clarity) in Fig. 1. In this figure, the peaks corresponding to the cobaltite phase have been indexed in agreement with previously reported data,[18] while the peak at around 28.5 degrees, marked by a ⋆, corresponds to the $BiBaO_3$ secondary phase with $Fm\bar{3}m$ space group (#225).[19] From this figure, it is clear that 222 phase is the major one in 15 mm/h grown samples. However, when the growth rate is increased, 222 peaks intensity are reduced while $BiBaO_3$ ones are increased (from Fig 1a to 1c). This trend can be easily seen when observing the relative intensity between the peaks found at about 28.5 and 29.0 degrees, indicating that higher growth speeds reduce the amount of 222 phase and increase $BiBaO_3$ secondary phases proportion. This evolution can be explained by the increase on the solidification rate when the growth speed is raised. As a consequence, solidification is produced out-of-equilibrium conditions leading to the formation of higher number of secondary phases.

SEM micrographs, performed on polished longitudinal sections for each growth speed, are displayed in Fig. 2. They show that samples possess very low porosity which slightly increases with the growth speed (small black spots in Fig. 2a-c, indicated by P). Furthermore, the amount of secondary phases is raised with the growth rate while the grain sizes and orientation are decreased, in clearly agreement with the XRD data. The different phases in the samples have been associated, through EDS, with the different contrasts found in the micrographs, indicated with arrows and numbers in Fig. 2 and summarized in Table I. Grey contrast (#1) has been identified as the thermoelectric Co-deficient 222 phase which is ~ 78 vol.% in samples grown at 15 mm/h, decreasing for

higher growth speeds until around 59 vol.% for the ones grown at 90 mm/h. Dark grey contrast (#2) corresponds to the $Ba_2Co_3O_y$ phase which follows the same trends observed for the 222 phase (from 6 to 2 vol.%). On the other hand, non thermoelectric secondary phases which can be observed as white (#3) and black contrasts (#4,) with $Bi_3Ba_2O_z$ and CoO compositions, respectively, raise their relative proportions in a very important manner (from 15 to 28 and 0.5 to 10 vol.%, respectively). These changes can be associated to the modification on the solidification rate discussed previously. Moreover, higher growth rates produce a higher number of nucleation centres which lead to lower grain sizes (see Fig. 2).

In order to study the effect produced by these microstructural changes on the thermoelectric properties, the temperature dependence of the electrical resistivity, as a function of growth rate, has been measured and represented in Fig. 3. In this figure it can be clearly seen that room temperature resistivity is decreased when the growth rates are reduced which confirms the higher grain size and orientation found in samples grown at lower rates. When considering the general resistivity behaviour as a function of temperature, samples grown at 90 mm/h show a marked semiconducting-type response with temperature. On the other hand, only slight semiconducting-like behaviour is found for samples grown at 30 mm/h while it is nearly temperature-independent in samples grown at 15 mm/h. In any case, the lowest resistivity values correspond to the 15 mm/h grown samples, in all the measured temperature range. These changes are mainly due to two main factors: first, reduction on the number and proportion of secondary phases, and second, increase of the gain size and alignment when the growth rate is reduced. Both factors lead to an important reduction on the resistivity values, reaching around 17 $m\Omega.cm$ at room temperature for samples grown at 15 mm/h which is slightly higher than the best reported values, around 6 $m\Omega.cm$.[21]

In Fig. 4 it is presented the Seebeck coefficient variation with temperature for the samples grown at different rates. In all the cases, S is positive in the whole range of measured temperatures, indicating a predominating hole-conduction mechanism. When comparing the S values at room temperature, it can be observed that they follow a parallel evolution with the electrical resistivity, they decrease with the growth rates. This effect is due to the same factors responsible for the electrical resistivity reduction, as

explained in the precedent paragraph. However, the measured S values are ranging from 125 μV/K to 145 μV/K for samples grown at 15 and 90 mm/h, respectively, which are higher than best reported value for this material, around 90 μV/K at room temperature.[21] Furthermore, S values increase from room temperature until they reach a maximum at about 300 ºC, decreasing at higher temperatures for samples grown at 90 mm/h. The same behaviour is found for those samples grown at 15 and 30 mm/h, which reach their maximum values at around 400 ºC and a less-marked decrease. The highest value at 650 ºC has been found to be ~ 150 μV/K for the 90 mm/h grown sample around 140% higher than the best reported one for this composition at the same temperature (around 110 μV/K).[22] The reason for obtaining such high S values in the LFZ grown samples, with respect to those obtained on samples prepared using conventional synthetic routes, is due to the formation of considerable amounts of oxygen vacancies on the thermoelectric phase when samples are textured using the LFZ technique.[23,24] This effect has also been observed in the misfit phase $[Ca_2CoO_3][CoO_2]_{1.62}$ which contains considerable amounts of oxygen vacancies when it is thermally treated under reducing atmosphere.[25] The raise on the oxygen vacancies changes the Co oxidation state from Co^{4+} to Co^{3+}, thus increasing S values, in agreement with Koshibae equation.[26]

In order to evaluate the thermoelectric performances of textured $Bi_2Ba_2Co_2O_x$ ceramic materials, variation of Power Factor with temperature has been calculated from the resistivity and Seebeck coefficient values and displayed, as a function of the growth rate, in Fig. 6. As a consequence of the important decrease on the resistivity with the growth rate, PF increases from about 0.01 $mW/K^2.m$ at room temperature for samples grown at 90 mm/h, to around 0.09 $mW/K^2.m$ for those textured at 15 mm/h. The maximum value obtained in these samples, ~ 0.16 $mW/K^2.m$ at 650 ºC, is about 4 times higher than the best previously reported values for this composition (0.04 $mW/K^2.m$ at 650 ºC).[22]

IV. CONCLUSIONS

This paper demonstrates that $Bi_2Ba_2Co_2O_X$ thermoelectric ceramics can be successfully grown using the laser floating zone (LFZ) technique. It has been determined that lower

growth rates lead to higher grain alignment and sizes and, as a consequence to lower electrical resistivity values. Seebeck coefficient decreases with the growth rate but, in any case, the obtained values are higher than the previously reported in the literature. The highest power factor value at 650 ºC for samples grown at 15 mm/h, around 0.16 mW/K^2m, is about 4 times higher than the best reported values for this composition. All these results make this textured material a promising candidate for practical applications in power generation systems.

IV. Acknowledgements

This research has been supported by the Spanish Ministry of Science and Innovation (Project MAT2008-00429) and the Universidad de Zaragoza (UZ2011-TEC-03). The authors wish to thank the Gobierno de Aragón (Consolidated Research Groups T12 and T87) for financial support, and to C. Gallego, C. Estepa and J. A. Gomez for their technical assistance. Sh. Rasekh acknowledges a JAE-PreDoc 2010 grant from the MICINN-CSIC.

References

1. Rowe DM. In: Rowe DM, editor. Thermoelectrics handbook: macro to nano. 1st ed. Boca Raton, FL: CRC Press; 2006. p. 1-3–7.

2. I. Terasaki, Y. Sasago, and K. Uchinokura, Phys. Rev. B 56,12685 (1997).

3. Funahashi R, Matsubara I, Ikuta H, Takeuchi T, Mizutani U, Sodeoka S. An oxide single crystal with high thermoelectric performance in air. Jpn J Appl Phys 2000;39:L1127–9.

4. Masset AC, Michel C, Maignan A, Hervieu M, Toulemonde O, Studer F, et al. Misfit-layered cobaltite with an anisotropic giant magnetoresistance: $Ca_3Co_4O_9$. Phys Rev B 2000;62:166–75.

5. Leligny H, Grebille D, Perez O, Masset AC, Hervieu M, Raveau B. A five-dimensional structural investigation of the misfit layer compound $[Bi_{0.87}\ SrO_2\ ]_2\ [CoO_2\ ]_{1.82}$. Acta Crystallogr B 2000;56:173–83.

6. Maignan A, Pelloquin D, Hébert S, Klein Y, Hervieu M. Thermoelectric power in misfit cobaltites ceramics: optimization by chemical substitutions. Bol Soc Esp Ceram V 2006;45:122–5.

7. Kobayashi W, Hebert S, Muguerra H, Grebille D, Pelloquin D, Maignan A. Thermoelectric properties in the misfit-layered-cobalt oxides [Bi(2)A(2)O(4)] [CoO2](b1/b2) (A = Ca, Sr, Ba, b(1)/b(2) = 1.65, 1.82, 1.98) single crystals. In: Kim I, editor. Proceedings ICT 07: twenty-sixth international conference on thermoelectrics. 2008. p. 117–20.

8. Maignan A, Hébert S, Hervieu M, Michel C, Pelloquin D, Khomskii D. Magnetoresistance and magnetothermopower properties of Bi/Ca/Co/O and Bi(Pb)/Ca/Co/O misfit layer cobaltites. J Phys: Condens Matter 2003;15:2711–23.

9. Zhang FP, Lu QM, Zhang JX. J Alloy Compd 2009;484:550.

10. Itahara H, Xia C, Sugiyama J, Tani T. Fabrication of textured thermo- electric layered cobaltites with various rock salt-type layers by using b-$Co(OH)_2$ platelets as reactive templates. J Mater Chem 2004;14:61– 6.

11. Guilmeau E, Mikami M, Funahashi R, Chateigner D. Synthesis and thermoelectric properties of $Bi_{2.5}Ca_{2.5}Co_2O_x$ layered cobaltites. J Mater Res 2005;20:1002–8.

12. Masuda Y, Nagahama D, Itahara H, Tani T, Seo WS, Koumoto K. J Mater Chem

2003;13:1094.
13. Nan J, Wu J, Deng Y, Nan C-W. Solid State Commun 2002;124:243.
Zhang FP, Lu QM, Zhang JX. J Alloy Compd 2009;484:550.
14. Diez, J. C., Rasekh, Sh., Madre, M. A., Guilmeau, E., Marinel, S., Sotelo, A. Improved thermoelectric properties of Bi-M-Co-O (M = Sr, Ca) misfit compounds by laser directional solidification. J. Electronic Mater. **39**, 1601-1605 (2010).
15. A. Sotelo, E. Guilmeau, Sh. Rasekh, M. A. Madre, S. Marinel, J. C. Diez. Enhancement of the thermoelectric properties of directionally grown Bi-Ca-Co-O through Pb for Bi substitution. J. Eur. Ceram. Soc. **30**, 1815-1820 (2010).
16. A. Sotelo, Sh. Rasekh, E. Guilmeau, M. A. Madre, M. A. Torres, S. Marinel, J. C. Diez. Improved thermoelectric properties in directionally grown $Bi_2Sr_2Co_{1.8}O_y$ ceramics by Pb for Bi substitution. Mater. Res. Bull. **46**, 2537-2542 (2011).
17. G. F. de la Fuente, J. C. Diez, L. A. Angurel, J. I. Peña, A. Sotelo, and R. Navarro: Wavelength dependence in laser floating-zone processing – A case study with Bi-Sr-Ca-Cu-O superconductors. Adv. Mater. 7, 853 (1995)
18. K. Sakai, T. Motohashi, M. Karppinen, H. Yamauchi: Enhancement in thermoelectric characteristics of the misfit-layered cobalt oxide, $[(Bi,Pb)_2Ba_{1.8}Co_{0.2}O_{4\pm\omega}]_{0.5}CoO_2$, through Pb-for-Bi substitution. Thin Solid Films 486 58 2005
19. Kennedy, B.J.; Howard, C.J.; Knight, K.S.; Zhang Zhao Ming; Zhou Qing Di. Structures and phase transitions in the ordered double perovskites $Ba_2Bi(III)Bi(V)O_6$ and $Ba_2Bi(III)Sb(V)O_6$. Acta Crystallographica B **62**, 537-546 (2006).
20. R. Ang, Y. P. Sun, X. Luo, and W. H. Song: A narrow band contribution with Anderson localization in Ag-doped layered cobaltites $Bi_2Ba_3Co_2O_y$, J. Appl. Phys. **102**, 073721 (2007).
21. H. Hao, H. Yang, Y. Liu, X. Hu: High-temperature thermoelectric properties of Cu-substituted $Bi_2Ba_2Co_{2-x}Cu_xO_y$ oxides. J. Mater. Sci. Technol. **27**, 525-528 (2011).
22. J.C. Diez, E. Guilmeau, M.A. Madre, S. Marinel, S. Lemonnier, A. Sotelo: Improvement of $Bi_2Sr_2Co_{1.8}O_x$ thermoelectric properties by laser floating zone texturing, Solid State Ionics180, 827, 2009
23. A. Sotelo, E. Guilmeau, M. A. Madre, S. Marinel, S. Lemmonier, J. C. Diez. $Bi_2Ca_2Co_{1.7}O_x$ thermoelectric ceramics textured by laser floating zone method. Bol. Soc.

Esp. Ceram. V. **47**, 225-228 (2008).
24. M. Karppinen, H. Fjellvåg, T. Konno, Y. Morita, T. Motohashi, H. Yamauchi, Chem. Mater. 16 (2004) 2790.
25. W. Koshibae, K. Tsutsui, and S. Maekawa: Thermopower in cobalt oxides, Physical Review B, V. 62, No. 11, 2000

Figure captions

Figure 1. XRD plots of the textured specimens obtained at different growth rates. a) 15; b) 30; and c) 90mm/h. The peaks corresponding to the $Bi_2Ba_2Co_2O_x$ thermoelectric phase are indexed while * indicates the $BiBaO_3$ secondary phase.

Figure 2. Scanning electron micrographs from longitudinal polished samples obtained with different growth rates: a) 15; b) 30; and c) 90 mm/h. The arrows indicate the different contrasts. #1, grey contrast (Co-deficient 222 phase); #2, dark grey ($Ba_2Co_3O_y$); #3, white ($Bi_3Ba_2O_z$); and #4 black one (CoO). P in the different micrographs is showing pores.

Figure 3. Temperature dependence of the electrical resistivity for samples grown at different rates: ● 15; ■ 30; and ◆ 90 mm/h.

Figure 4. Temperature dependence of the Seebeck coefficient for samples grown at different rates: ● 15; ■ 30; and ◆ 90 mm/h.

Figure 5. Temperature dependence of the power factor for samples grown at different rates: ● 15; ■ 30; and ◆ 90 mm/h.

Figure 1

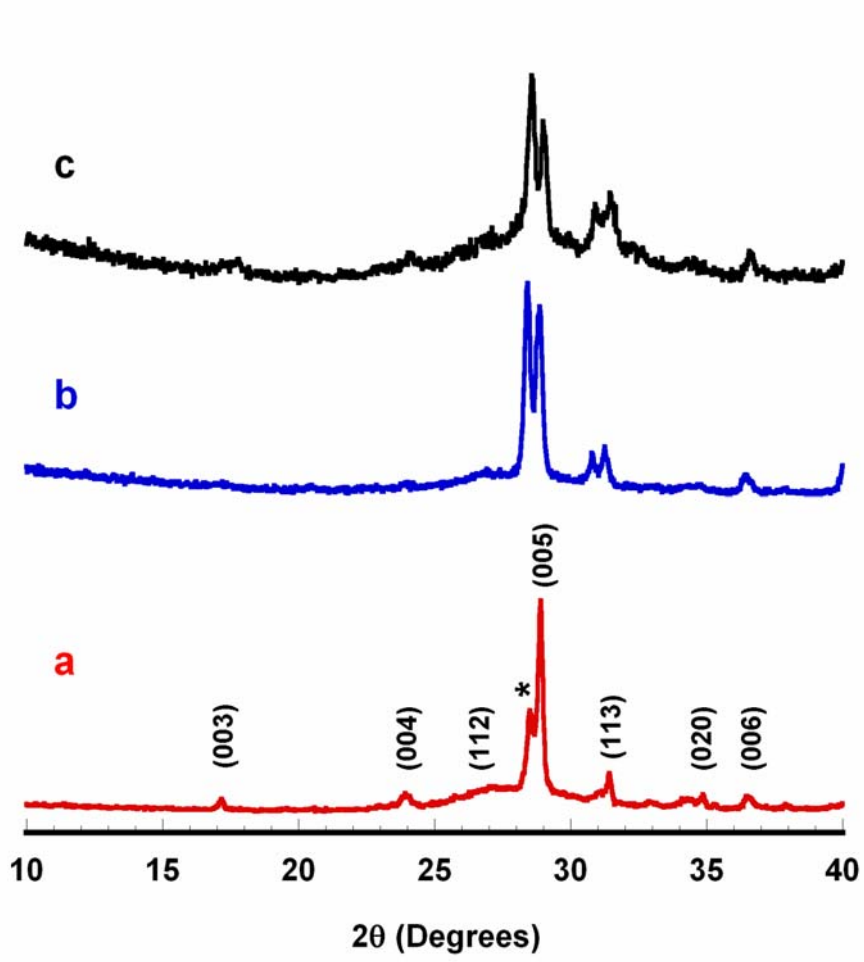

Figure 2

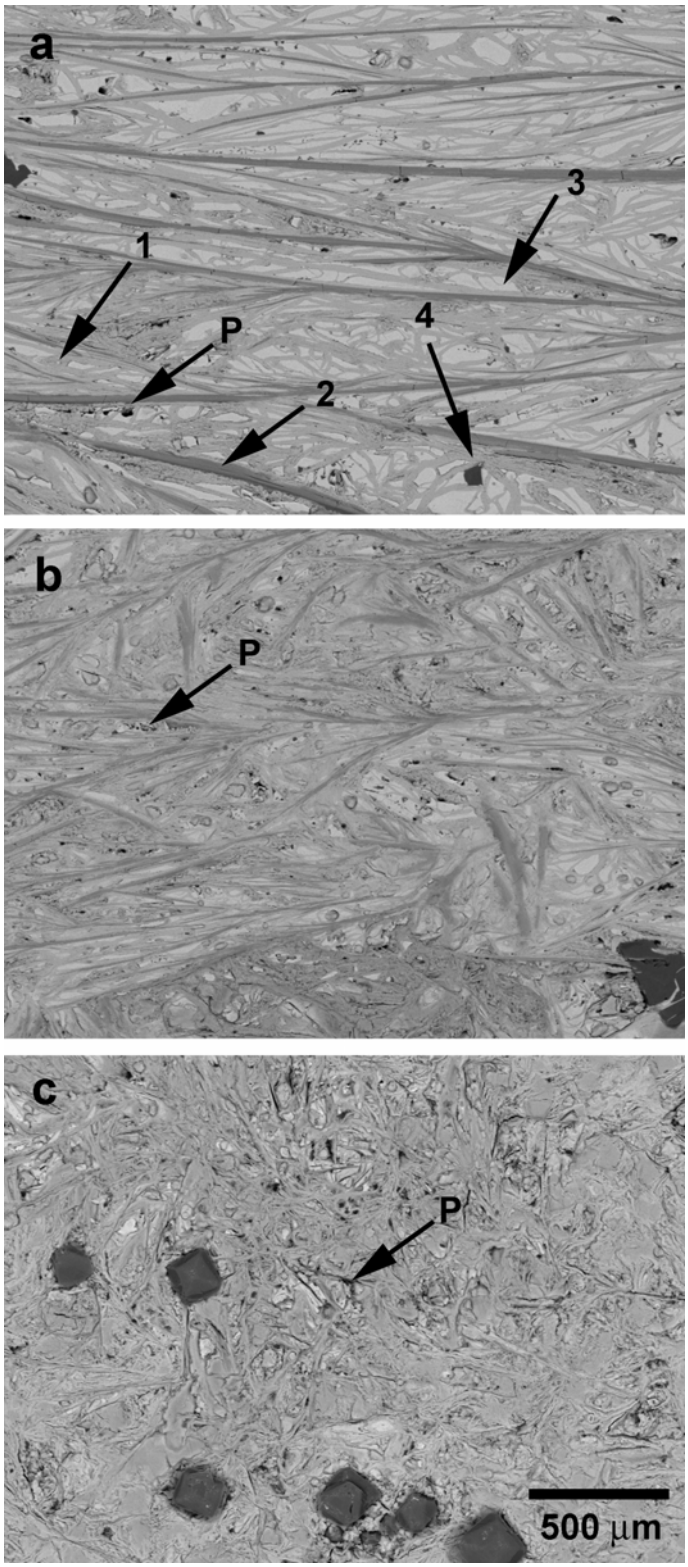

Figure 3

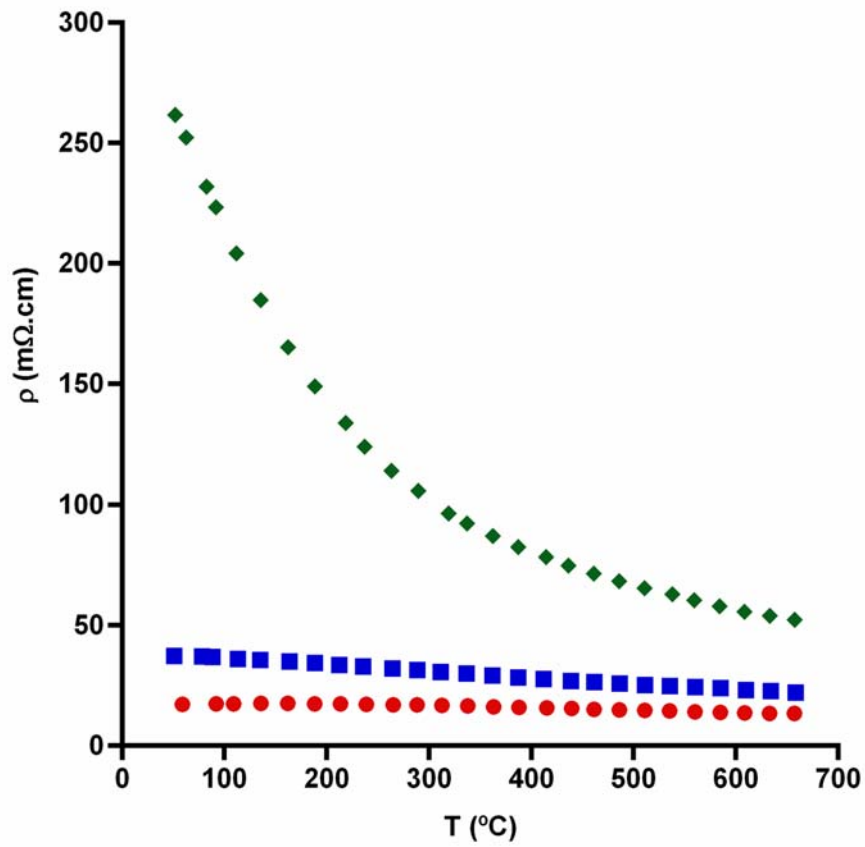

Figure 4

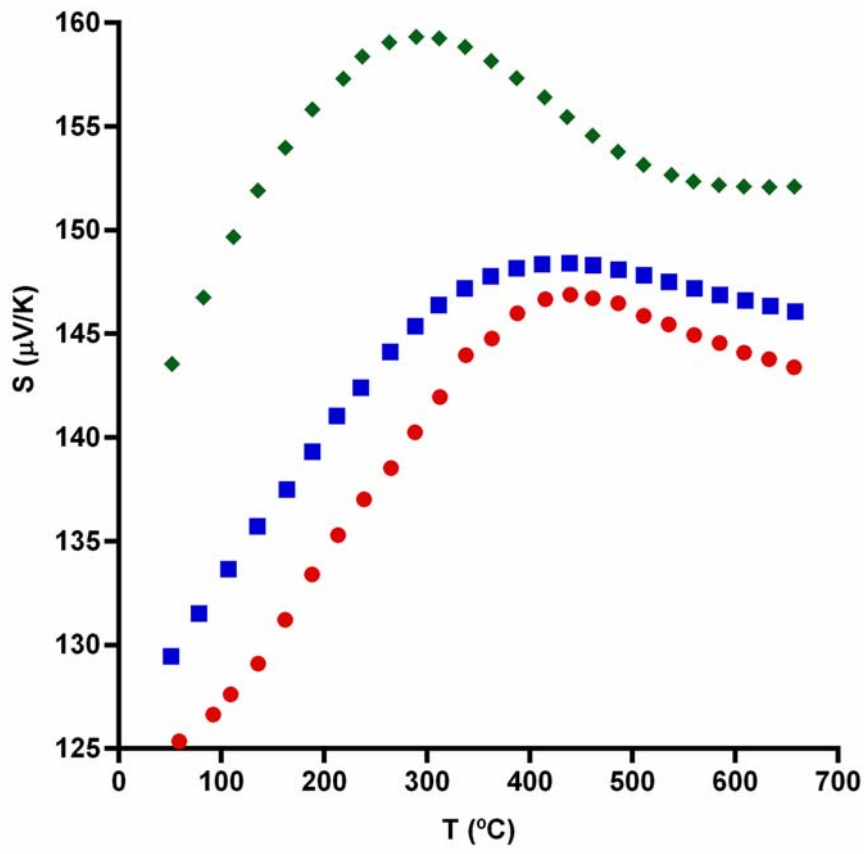
160
155
150
145
140
135
130
125
S (μV/K)
0
100
200
300
400
500
600
700
T (°C)

Figure 5